Successive Phase Transitions and High Ionic Conductivity of Trichlorogermanate(II) Salts as Studied by ^{35}Cl NQR and Powder X-Ray Diffraction*

K. Yamada, K. Isobe, T. Okuda

Department of Chemistry, Faculty of Science, Hiroshima University, Kagamiyama 1-3, Higashi-Hiroshima 724, Japan

Y. Furukawa

Faculty of School Education, Hiroshima University, Shinonome 3-1-33, Minami-ku, Hiroshima 734, Japan

Z. Naturforsch. **49a**, 258–266 (1994); received July 23, 1993

A series of trichlorogermanate(II) salts ($AGeCl_3$, A = Rb, Cs, CH_3NH_3, and $(CH_3)_4N$) have been synthesized and characterized by ^{35}Cl NQR, ^{35}Cl NMR, AC conductivity, DTA, and X-ray diffraction techniques. In the temperature range studied two, two, five, and four phases were confirmed for the Rb, Cs, CH_3NH_3, and $(CH_3)_4N$ salts, respectively. From the ^{35}Cl NQR and structural data, isolated pyramidal $GeCl_3^-$ anions were recognized in the low temperature phases. With increasing temperature the relaxation times of the ^{35}Cl NQR decreased exponentially and the signals disappeared far below the melting point. This suggests that the reorientation of the anion about the pseudo three-fold axis is excited. With further increase in temperature, the ionic conductivity of $CH_3NH_3GeCl_3$ and $(CH_3)_4NGeCl_3$ increased drastically at the phase transitions to their cubic perovskite phases ($CH_3NH_3GeCl_3$: $\sigma = 10^{-1}$ S m^{-1} at 400 K, $(CH_3)_4NGeCl_3$: $\sigma = 5 \times 10^{-2}$ S m^{-1} at 420 K). The mobile ion was confirmed to be the chloride ion by means of ^{35}Cl NMR and X-ray diffraction.

Key words: ^{35}Cl NQR, ^{35}Cl NMR, Ionic conductivity, Rietveld analysis, Phase transition.

Introduction

ABX_3 (A = alkaline metal and alkylammonium, B = Ge(II) and Sn(II), X = Cl, Br, and I) are an interesting group of compounds because of the changes of their structure and physical properties at the phase transition temperature. For example, a semiconductor to metal transition in $CsSnI_3$ ($T_{tr} = 425$ K) [1] and an insulator to semiconductor transition in $CH_3NH_3SnBr_3$ ($T_{tr} = 229$ K) [2] have been found. These phase transitions have been characterized by means of ^{127}I NQR, ^{119}Sn Mössbauer effect, and powder X-ray diffraction techniques [1–3], and by heat capacity measurements [4]. From these observations it is supposed that the electronic conductivity is greatly associated with the linear chain –X–Sn–X–Sn– existing in the perovskite lattice.

In this paper, we have examined the succesive phase transitions of a series of trichlorogermanate(II) salts by measuring ^{35}Cl NQR, ^{35}Cl NMR, X-ray diffraction, and AC conductivity. In this group of trichlorogermanate(II) salts, as opposed to the Sn(II) salts, drastic increases of ionic conductivity were observed for $CH_3NH_3GeCl_3$ and $(CH_3)_4NGeCl_3$, associated with the phase transitions to their cubic perovskite phases. It is interesting that both types of conductivity (electronic and ionic) have been found for the Sn and Ge compounds having perovskite structure. As is expected from the quite different electrical properties, the perovskite structure of the high ionic conductor is disordered. In the electronic conducting $CuSnI_3$ the linear chain –I–Sn–I–Sn– plays an important role and the conductivity decreases drastically if the bond distorts –Sn $\cdots$ X–Sn $\cdots$ X–, just like a Peierls transition. In the Ge(II) halides, having high ionic conductivity, the perovskite structure of $CH_3NH_3GeCl_3$ and $(CH_3)_4NGeCl_3$ appears; as a result of an averaged structure of the disordered state, i.e., Ge–X $\cdots$ Ge and Ge $\cdots$ X–Ge. This averaged structure is the reason for the high ionic conduc-

* Presented at the XIIth International Symposium on Nuclear Quadrupole Resonance, Zürich, July 19–23, 1993.

Reprint requests to Dr. Koji Yamada, Department of Chemistry, Faculty of Science, Hiroshima University, Kagamiyama 1-3, Higashi-Hiroshima 724, Japan.

0932-0784 / 94 / 0100-0258 $ 01.30/0. – Please order a reprint rather than making your own copy

tivity of the cubic phase. A possible mechanism for the ionic conductivity will be discussed on the basis of the dynamic and static structural information.

Both the electronic and ionic conductivity are closely related to the bonding property of the main group element having an s-electron lone pair, or in other words, the hypervalent nature of the central metal atom. That is, a symmetric 3c–4e (three-center-four-electrons) bond, X–M–X, found in the cubic perovskite structure, tends to deform asymmetrically X–M · · · X because of the weak covalent character of the bond [5–7].

Experimental

Sample Preparation

$AGeCl_3$ (A = Rb, Cs, CH_3NH_3, and $(CH_3)_4N$) were prepared from equimolar amounts of ACl and germanium(II) hydroxide in 6 N hydrochloric acid [8]. Germanium(II) hydroxide was synthesized in advance from germanium(IV) oxide as previously described [9, 10]. The samples were recrystallized from the mixed solvent of methyl alcohol and hydrochloric acid (1:1) and then dried in vacuo at room temperature. In the case of $RbGeCl_3$, $CsGeCl_3$ and $(CH_3)_4NGeCl_3$, samples were identified by Powder X-ray diffraction comparing with the simulated patterns [11–15]. The analytical data are as follows. Found: C, 5.69; H, 2.87; N, 6.64%. Calcd. for $CH_3NH_3GeCl_3$: C, 5.43; H, 2.67; N, 6.63%. Found: C, 18.98; H, 4.78; N, 5.53%. Calcd. for $(CH_3)_4NGeCl_3$: C, 19.03; H, 4.84; N, 5.53%.

Measurements

^{35}Cl NQR spectra were observed by a Matec pulsed spectrometer in the temperature range from 77 K to disappearance temperature. ^{35}Cl NMR was detected only for the CH_3NH_3 analogue above ca. 360 K by means of the same Matec spectrometer applying a magnetic field of 6.37 T. The spin-lattice relaxation times of NQR were determined by a conventional pulse technique. The temperature dependence of the ionic conductivity was measured by means of a complex impedance method at 10 different frequencies (100 Hz ~ 100 kHz, ANDO LCR meter AG-4311) using a pressed powder disk coated by carbon or silver past on both sides. Powder X-ray diffraction patterns were obtained with a Rigaku and Rad-B system and a home built high-temperature attachment using Cu K_α radiation. The observed diffraction patterns were analyzed by Rietveld refinement using a Fortran program "RIETAN" [16]. Further experimental details on the Rietveld analysis are summarized in Table 1.

Results and Discussion

Successive Phase Transitions in the Series $MGeCl_3$

The phases and phase transition temperatures of these compounds are summarized in Figure 1, where

Table 1. Crystal data and experimental details of the Rietveld Refinements for $CsGeCl_3$ (Phase I and II), $CH_3NH_3GeCl_3$ (Phase II and III), and $(CH_3)_4NGeCl_3$ (Phase I and II).

Compounds	$CsGeCl_3$		$CH_3NH_3GeCl_3$		$(CH_3)_4NGeCl_3$	
Phase	I	II	II	III	I	II
Temperature/K	449	294	398	381	440	294
Crystal system	Cubic	Trigonal	Cubic	Trigonal	Cubic	Orthorhombic
Space group	Pm3m	R3m	Pm3m	R3m	Pm3m	Pnma
Lattice constant	$a = 5.478(1)$ Å	$a = 5.439(1)$ Å $\alpha = 89.71(1)^\circ$	$a = 5.658(1)$ Å	$a = 5.659(1)$ Å $\alpha = 90.90(1)^\circ$	$a = 6.547(1)$ Å	$a = 13.089(1)$ Å $b = 9.135(1)$ Å $c = 8.916(1)$ Å
d_{cal}/g cm^{-3}	3.150	3.219	1.935	1.934	1.498	1.577
Z	1	1	1	1	1	4
Number of parameters	18	22	16	23	16	28
2θ range/Degree	10–80	10–90	10–80	10–80	10–60	10–60
Step width/Degree	0.04	0.04	0.04	0.04	0.04	0.04
R_p [a]	0.136	0.094	0.110	0.103	0.107	0.083
R_F [b]	0.114	0.080	0.115	0.091	0.127	0.067
DS, RS, SS/Degree [c]	0.5, 0.15, 0.5	0.5, 0.15, 0.5	0.5, 0.15, 0.5	0.5, 0.15, 0.5	1.0, 0.3, 1.0	0.5, 0.15, 0.5

[a] $R_p = \sum |y_i(\text{obs}) - y_i(\text{cal})| / \sum y_i(\text{obs})$, where y_i (obs) and y_i (cal) are the observed and calculated intensity at ith step.
[b] $R_F = \sum |(I_K(\text{obs}))^{1/2} - (I_K(\text{cal}))^{1/2}| / \sum I_K(\text{obs})^{1/2}$, where I_K is the intensity assigned to the Kth Bragg reflection.
[c] Divergence slit, receiving slit, and scatter slit.

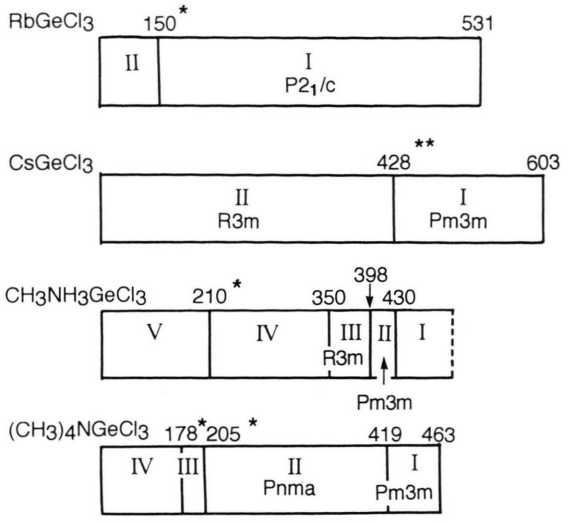

Fig. 1. Phase transitions of $AGeCl_3$ (A = Rb, Cs, CH_3NH_3, and $(CH_3)_4N$) determined by ^{35}Cl NQR (denoted by *), DTA, and X-ray diffraction pattern (**). Temperatures in K.

the transition temperatures (T_{tr}) were determined by ^{35}Cl NQR, DTA, and X-ray diffraction techniques. Below room temperature the transition temperatures were determined by the NQR frequency versus temperature graphs (Figs. 2 and 3). Above room temperature they were determined mainly by the DTA heating curves because of the disappearance of the NQR signal due to the reorientation of the $GeCl_3^-$ anion. Only the phase transition of $CsGeCl_3$ from trigonal to cubic could not be detected by DTA, but was confirmed by the temperature dependence of the X-ray diffraction pattern (Figure 7(B)). This transition temperature was in good agreement with the previous DTA measurement [13].

Temperature Dependence of the ^{35}Cl NQR Frequency and Spin-Lattice Relaxation Time

Figures 2 and 3 show the ^{35}Cl NQR frequencies in the range from 77 K to the disappearance temperature. In general, halogen NQR frequencies appear in a wide frequency range if the halogen is bonded to a hypervalent metal such as Sn(II), Ge(II), and Sb(III). This is because the covalent character of the X–M (X: halogen) bond strongly depends on the weak interaction M · · · X located at the *trans* position. This type of interaction is characteristic for hypervalent central elements, and an anion having a high ^{35}Cl NQR frequency is supposed to be more isolated.

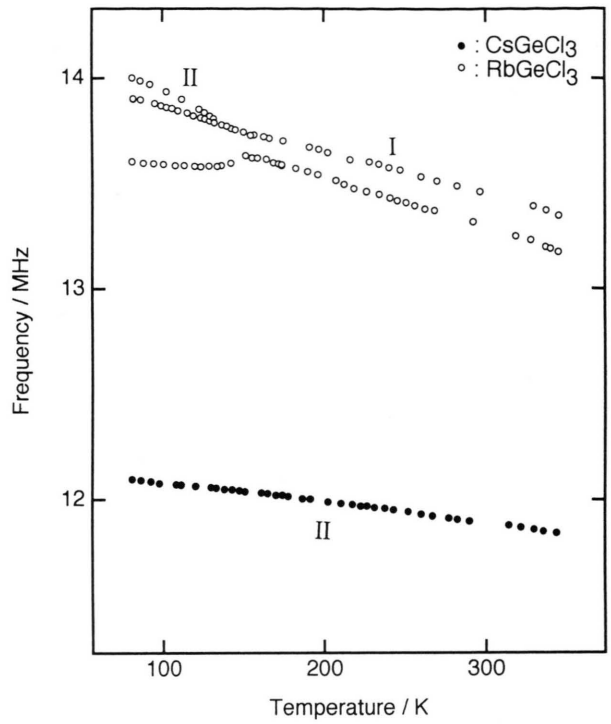

Fig. 2. Temperature dependence of the ^{35}Cl NQR frequency for $RbGeCl_3$ and $CsGeCl_3$.

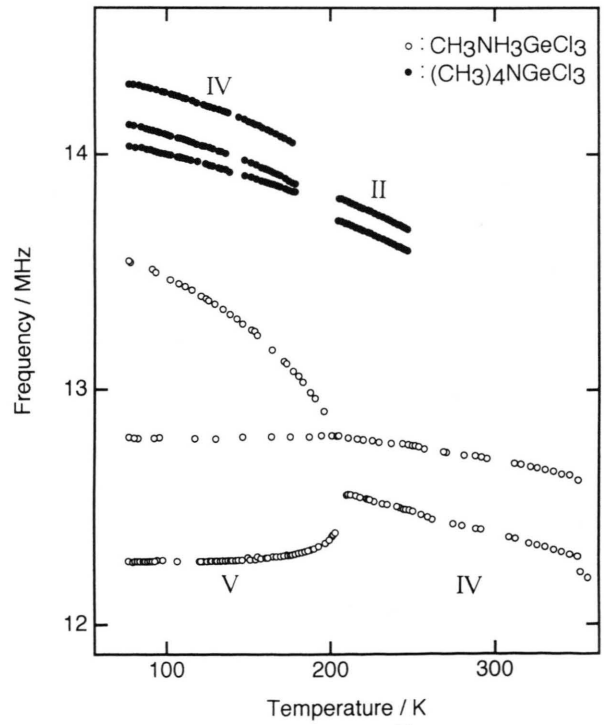

Fig. 3. Temperature dependence of the ^{35}Cl NQR frequency for $CH_3NH_3GeCl_3$ and $(CH_3)_4NGeCl_3$.

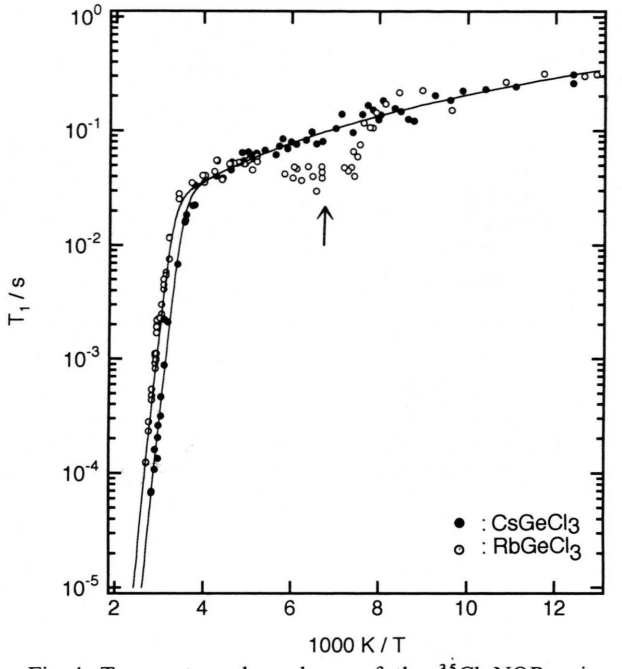

Fig. 4. Temperature dependence of the ^{35}Cl NQR spin-lattice relaxation time for $RbGeCl_3$ and $CsGeCl_3$. Arrow indicates the phase transition temperature as shown in Figs. 1 and 2.

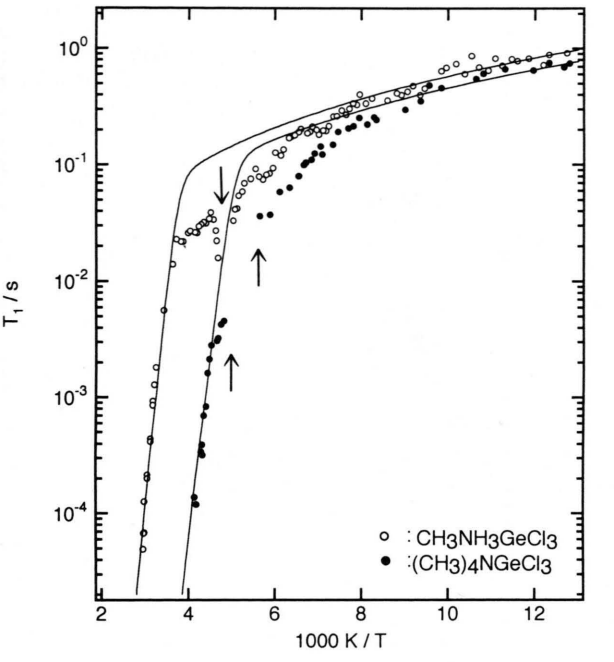

Fig. 5. Temperature dependence of the ^{35}Cl NQR spin-lattice relaxation time for $CH_3NH_3GeCl_3$ and $(CH_3)_4NGeCl_3$. Arrow indicates the phase transition temperature as shown in Figs. 1 and 3.

Compound	Frequency/MHz		a/s^{-1}	n	b/s^{-1}	E_a/kJ mol^{-1}
	77 K	292 K				
$RbGeCl_3$	14.113(1)[a] 13.917(1) 13.668(1)	13.462(1) 13.307(2)	7.7×10^{-4}	1.9 ± 0.1	4.2×10^{14}	76 ± 3
$CsGeCl_3$	12.094	11.892	7.7×10^{-4}	1.9 ± 0.1	1.2×10^{15}	74 ± 5
$CH_3NH_3GeCl_3$	13.550(1) 12.798(1) 12.270(1)	12.716(1) 12.409(2)	1.7×10^{-4} [b]	2.0	2.9×10^{15}	74 ± 5
$(CH_3)_4NGeCl_3$	14.301(1) 14.128(1) 14.035(1)		2.2×10^{-4} [b]	2.0	6.7×10^{16}	60 ± 5

Table 2. ^{35}Cl NQR frequencies and relaxation parameters of (1) for $AGeCl_3$ (A = Rb, Cs, CH_3NH_3, and $(CH_3)_4N$).

[a] Relative intensity in parentheses.

[b] Estimated below 100 K with fixed n value.

Figures 4 and 5 show the temperature dependence of the ^{35}Cl NQR spin-lattice relaxation times. All compounds studied showed abrupt decreases of the relaxation time and then the NQR signals disappeared far below the melting point, suggesting the onset of $GeCl_3^-$ reorientation around the pseudo three-fold axis. In general, the NQR relaxation rate $(1/T_1)_{obs}$ is expressed as a sum of the two contributions,

$$(1/T_1)_{obs} = a\,T^n + b\exp(-E_a/R\,T)\,, \qquad (1)$$

where first term represents the Raman process and the second term the reorientation of the fragment containing the nucleus monitored. Relaxation parameters, a, n, b, and E_a are summarized in Table 2. The temperature dependence of the relaxation times for $CsGeCl_3$

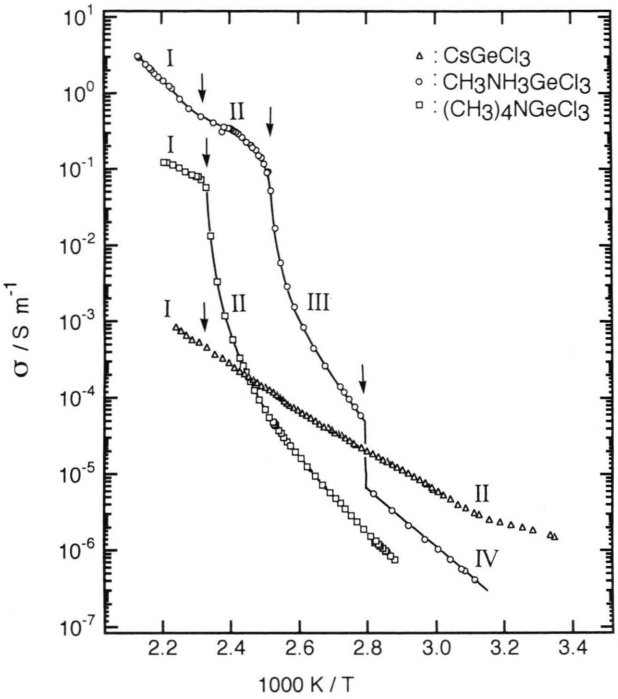

Fig. 6. Temperature dependence of the AC conductivity determined by means of the complex impedance method.

Table 3. Activation energy of the AC conductivity for $AGeCl_3$ (A = Cs, CH_3NH_3, and $(CH_3)_4N$).

Compound	Phase	Temp. Range/K	E_a/kJ mol^{-1}
$CsGeCl_3$	I, II	357–444	56
$CH_3NH_3GeCl_3$	II	415–425	ca. 33[a]
	IV	320–356	75
$(CH_3)_4NGeCl_3$	I	433–455	40
	II	344–384	88

[a] Linear portion was too small to estimate accurately.

and $RbGeCl_3$ could be expressed satisfactorily using the parameters in Table 2 except near phase transition temperature. For $CH_3NH_3GeCl_3$ and $(CH_3)_4NGeCl_3$, on the other hand, the T_1 deviated from (1) over a wide temperature range suggesting contributions from the modulation effect of the cation dynamics and/or from the second order phase transition.

Temperature Dependence of the AC Conductivity

Figure 6 shows the temperature dependence of the AC conductivity above room temperature. In $CsGeCl_3$ there is no pronounced increase in the conductivity at

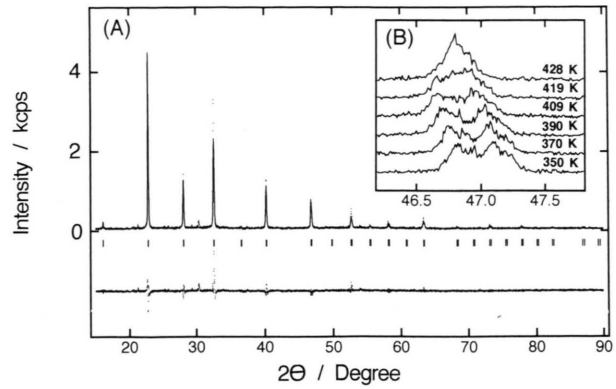

Fig. 7. Powder X-ray diffraction pattern of $CsGeCl_3$ observed at (A) 428 K (Phase I, Cubic Pm3m) and (B) near the phase transition temperature from the trigonal to cubic phase. Two trigonal (220) and (−220) Bragg reflections merged into (220) reflection at 428 K.

the transition from the trigonal to the cubic phase. In $CH_3NH_3GeCl_3$ and $(CH_3)_4NGeCl_3$, on the other hand, abrupt increases of the conductivity have been found just below the phase transition to their cubic phases. Table 3 summarizes activation energies according to the Arrhenius equation

$$\sigma = A \exp(-E_a/RT), \tag{2}$$

determined from the linear portion of the $\ln\sigma$ vs. $1/T$ graph. The activation energies for $CH_3NH_3GeCl_3$ and $(CH_3)_4NGeCl_3$ in their cubic phases decrease to about one-half of their value in the room temperature phases. This suggests a disordered structure in the cubic phase.

Powder X-ray Diffraction and Rietveld Refinement

1.) $CsGeCl_3$: As is expected from the single ^{35}Cl NQR line, Phase II at 293 K was confirmed to be a trigonal with space group R3m by the Rietveld refinement (Table 1). This is consistent with the single crystal data reported by Thiele [12]. With increasing temperature several Bragg reflections merged into singlets as shown in Fig. 7(B), suggesting a phase transition to a cubic system at 428 K. Although for some peaks (for example (200) and (310) reflections) the difference between observed and calculated intensity was not satisfactorily small in the cubic phase (Phase I), any disordered structure, such as found in $CH_3NH_3GeCl_3$ or $(CH_3)_4NGeCl_3$, could not be confirmed. These findings are consistent with the temperature dependence of the AC conductivity, in which no abrupt increase in

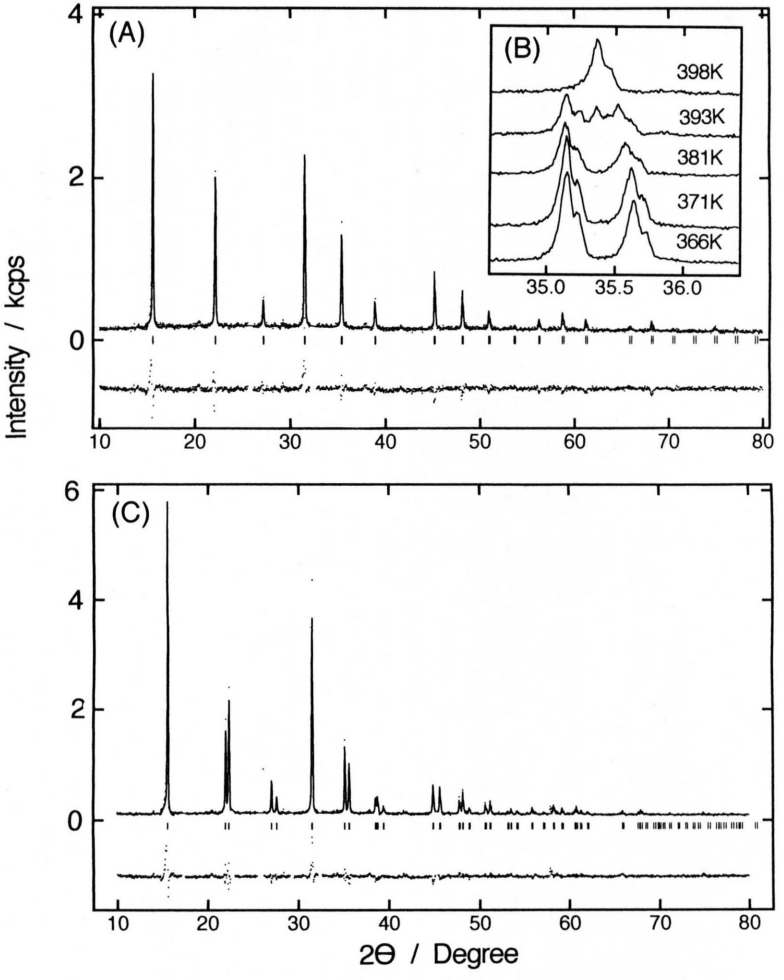

Fig. 8. X-ray diffraction pattern of $CH_3NH_3GeCl_3$. (A) Final Rietveld refinement plot of phase II observed at 398 K. Solid-line: calculated pattern, dots: observed. The lower portion shows the difference between them. (B) Typical changes of the diffraction pattern near the phase transition temperature from the trigonal to cubic phase. (C) Final Rietveld refinement of the trigonal phase observed at 381 K.

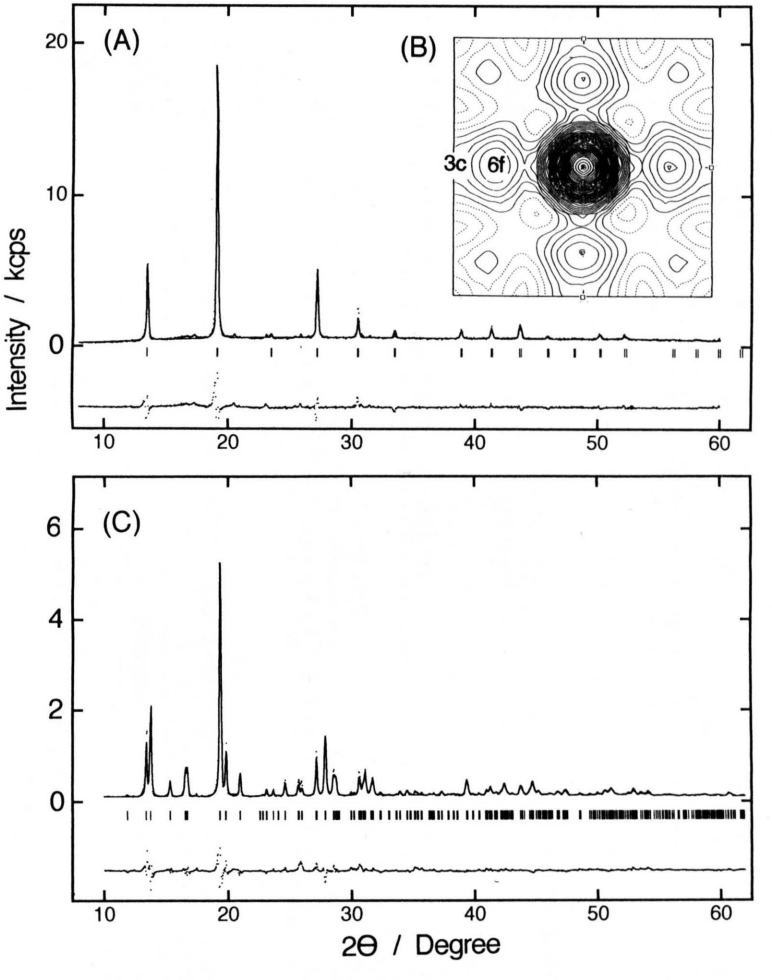

Fig. 9. X-ray diffraction pattern of $(CH_3)_4NGeCl_3$. (A) Final Rietveld refinement plot of phase I observed at 398 K. (B) Fourier synthesis at $Z=0.5$ calculated from the observed F_0 and calculated phase. (C) Final Rietveld refinement of the orthorhomic phase (Phase II) observed at 294 K.

Table 4. Positional and isotropic thermal parameters of $CsGeCl_3$ (Phase II at 294 K) and $CH_3NH_3GeCl_3$ (Phase II at 398 K and Phase III at 381 K) with estimated standard deviations in parentheses.

Phase	Atom	Position[a]	Occupation	x	y	z	$B_{iso}/Å^2$
II(R3m)	Cs	1a, 3m	1	0	0	0	5.4(8)
	Ge	1a, 3m	1	0.495(5)	$=x$	$=x$	0.8(8)
	Cl	3b, m	1	0.519(6)	$=x$	0.052(7)	7.7(18)[c]
II(Pm3m)	CH_3NH_3[b]	1a, m3m	1	0	0	0	30.8(53)
	Ge	1b, m3m	1	0.5	0.5	0.5	5.8(15)
	Cl	6f, 4mm	0.5	0.069(13)	0.5	0.5	7.4(26)
III(R3m)	CH_3NH_3[b]	1a, 3m	1	0	0	0	32.4(31)
	Ge	1a, 3m	1	0.495(17)	$=x$	$=x$	6.5(12)
	Cl	3b, m	1	0.486(18)	$=x$	0.914(17)	10.1(18)[c]

[a] Wyckoff notation and point symmetry.
[b] Isoelectronic K^+ was used for the refinement instead of $CH_3NH_3^+$.
[c] Isotropic thermal parameter was calculated from an anisotropic parameters, $\beta_{11}=\beta_{22}=0.042(12)$, $\beta_{33}=0.005(10)$, $\beta_{12}=\beta_{13}=-0.014(14)$, and $\beta_{23}=0.001(20)$ for $CsGeCl_3$. $\beta_{11}=\beta_{22}=0.086(16)$, $\beta_{33}=0.022(20)$, $\beta_{12}=\beta_{13}=0.004(8)$, and $\beta_{23}=0.003(17)$ for $CH_3NH_3GeCl_3$.

Table 5. Positional and isotropic thermal parameters of $(CH_3)_4NGeCl_3$ at 440 K (Phase I) and 294 K (Phase II) with estimated standard deviations in parentheses.

Phase	Atom	Position[a]	Occupation	x	y	z	$B_{iso}/Å$
I(Pm3m)	$(CH_3)_4N$[b]	1a, m3m	1	0	0	0	58.6(58)
	Ge	1b, m3m	1	0.5	0.5	0.5	9.8(30)
	Cl	6f, 4mm	0.5	0.158(15)	0.5	0.5	15.7(60)
II(Pnma)	$(CH_3)_4N$[b]	4c, m	1	0.5020(19)	0.25	0.2406(31)	83.9(12)
	Ge	4c, m	1	0.7604(8)	0.25	0.7507(10)	5.1(4)
	Cl	4c, m	1	0.9256(15)	0.25	0.8045(22)	9.2(5)
	Cl	8d, 1	1	0.7520(15)	0.0619(12)	0.5806(13)	7.0(5)

[a] Wyckoff notation and point symmetry.
[b] Isoelectronic dummy atom Tc was used for the refinement.

the conductivity was found at the phase transition temperature.

2.) $CH_3NH_3GeCl_3$: As far as we know, there is no crystal structural report on this sample. The preliminary analysis of the powder X-ray diffraction pattern at 294 K (Phase IV) suggested that the crystal belongs to an orthorhombic system with space group Pnma and is isomorphous with $(CH_3)_4NGeCl_3$ as described later. A determination of the precise structural parameters of Phase IV is now in progress. With increasing temperature it transformed into a simple trigonal powder pattern as shown in Fig. 8(C). With further increasing temperature, it turns to a cubic phase (Phase II). Another phase was found above 430 K without apparent diffraction peak. We tentatively assigned this totally disordered highest temperature phase as Phase I. Table 4 lists the positional parameters for Phases II and III together with that of the Cs analogue. It is particularly interesting that the cubic phase (Phase II) is a *disordered* perovskite in which Cl atoms occupy 6f sites with 50% probability instead of the original 3c sites. Satisfactory R parameters could be obtained only by adopting this disorder model.

3.) $(CH_3)_4NGeCl_3$: This compound was reported to be an orthorhombic system with space group $Pna2_1$ at room temperature (Phase II) [14]. However, we adopted space group Pnma for the Rietveld refinement because two ^{35}Cl NQR lines with intensity ratio 1:2 were observed for Phase II (Figure 3). Final parameters and powder pattern are shown in Table 5 and Figure 9, respectively. The Ge–Cl bond length is considerably shorter than the Ge · · · Cl bond located at the *trans* position (Ge–Cl: 2.27 Å, Ge · · · Cl: 4.20 Å on the average). This suggests that an isolated $GeCl_3^-$ anion exists in Phase II, although the perovskite structure is kept essentially as shown in Figure 10. With increasing temperature the X-ray diffraction pattern changed drastically above 419 K and gave a simple

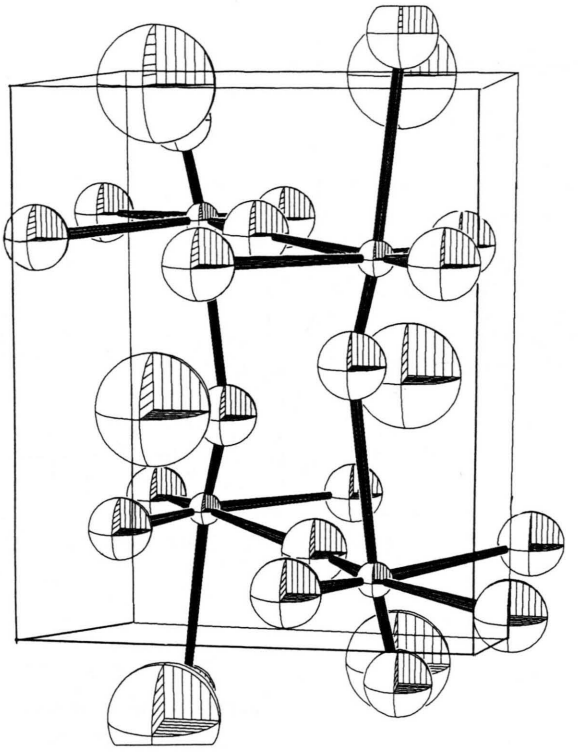

Fig. 10. ORTEP drawing of $(CH_3)_4NGeCl_3$ at 294 K (Phase II).

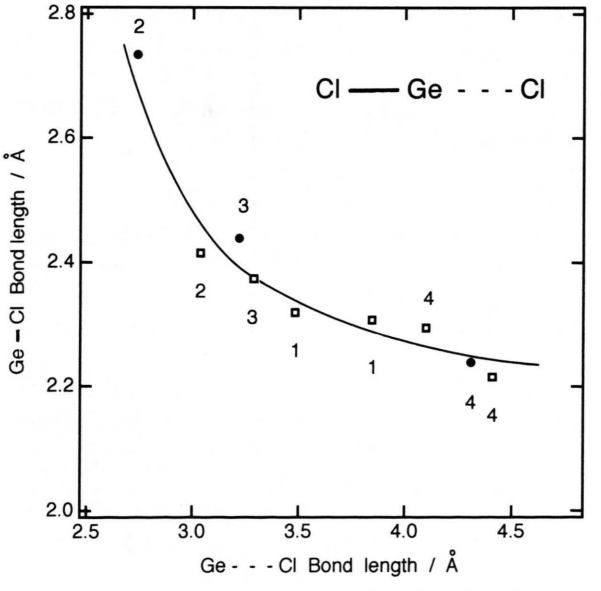

Fig. 11. The Ge–Cl bond length is plotted against the *trans* Ge · · · Cl bond length. Circles correspond to cubic phases and squares to lower temperature phases. 1: $RbGeCl_3$, 2: $CsGeCl_3$, 3: $CH_3NH_3GeCl_3$, and 4: $(CH_3)_4NGeCl_3$.

Table 6. Ge–Cl Bond length together with the Ge · · · Cl bond located at the *trans* position.

Compound	Phase	Ge–Cl/Å	Ge · · · Cl/Å
$RbGeCl_3$	II[a]	2.307	3.874
		2.319	3.482
$CsGeCl_3$	I	2.735	2.735
	II	2.348	3.092
$CH_3NH_3GeCl_3$	II	2.439	3.219
	III	2.374	3.287
$(CH_3)_4NGeCl_3$	I	2.239	4.308
	II	2.215	4.410
		2.294	4.098

[a] See Ref. (11).

diffraction pattern which could be indexed as cubic. Although the observed intensity could not be simulated from an ideal perovskite structure, satisfactorily good R parameters were obtained with a disordered model, similar to $CH_3NH_3GeCl_3$, where the Cl atoms are located at the 6f site with an occupation factor, of 50% as shown in Table 5. Figure 9(B) shows a fourier map at $z = 0.5$, in which Ge and four Cl sites are clearly seen. This type of disorder was first suggested by Depmeier [14]. This disorder is quite different from that found in ionic conducting perovskite such as $CsPbCl_3$ [17–20].

The Ge–Cl bond lengths are summarized in Table 6 together with the Ge · · · Cl bonds located at the *trans* positions, and are plotted in Figure 11. It is interesting that the relation between the bond lengths is valid not only for the low temperature phase but also for the disordered cubic phases. From this it becomes apparent that the ideal perovskite structure is impossible for $(CH_3)_4NGeCl_3$ because the symmetric Cl–Ge–Cl bond is too long to exist in the cubic lattice.

^{35}Cl NMR and a Possible Mechanism for the High Ionic Conductivity

Figure 12 shows the ^{35}Cl NMR line of $CH_3NH_3GeCl_3$ above 364 K. With increasing temperature the NMR signal became sharp, its intensity increased and was clearly observable in Phases II and I. It should be emphasized that the quadrupole coupling constant for ^{35}Cl is about 25 MHz, which is comparable to the Larmor frequency of the ^{35}Cl NMR in our experimental condition. This finding suggests that the correlation frequency of the Cl^- self-dif-

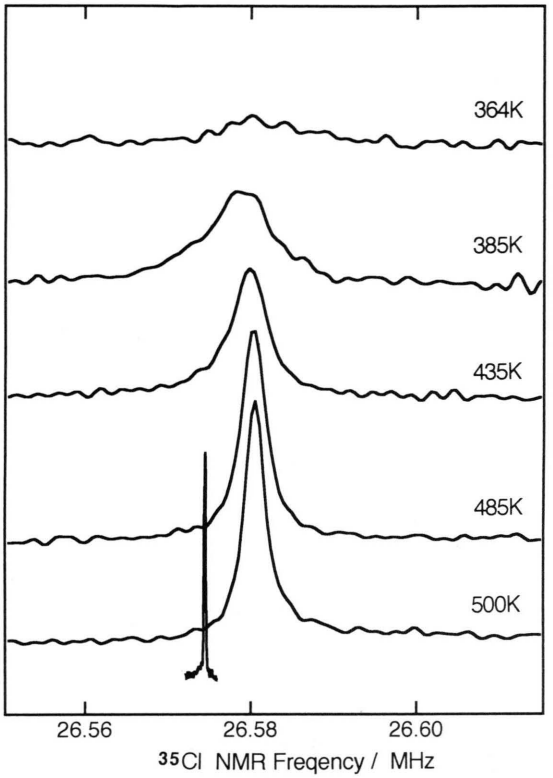

Fig. 12. Temperature dependence of the ^{35}Cl NMR spectra of $CH_3NH_3GeCl_3$ detected above 364 K. The sharp signal at the bottom is a ^{35}Cl NMR signal of powdered KCl.

fusion, $1/\tau_c$, is much higher than the quadrupole coupling constant ($1/\tau_c \gg e^2 Q q/h$) and the ^{35}Cl nucleus sees an almost zero quadrupole coupling constant. A mechanism is proposed for the Cl^- self-diffusion on

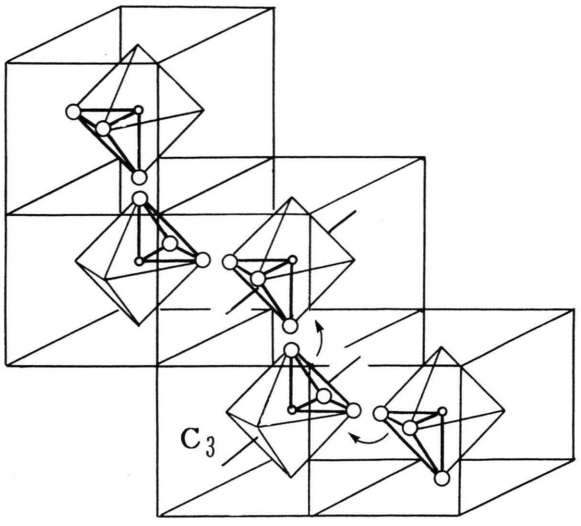

Fig. 13. One of the possible diffusion paths for the chloride ion in the cubic perovskite lattice.

the basis of the disordered structure (cf. Fig. 13). It consists of two processes, translational jumps between 6f sites and $GeCl_3^-$ reorientation around the C_3 axis. Since the chlorine atoms occupy statistically the 6f sites with equal probabilities, the time-averaged efg vanishes to zero in accord with our observation if the condition $1/\tau_c \gg e^2 Q q/h$ is retained. The cubic perovskite structure of $CH_3NH_3GeCl_3$ and $(CH_3)_4NGeCl_3$ is a dynamic disordered one, in which first switching of the bonds, Cl–Ge · · · Cl and Cl · · · Ge–Cl, and reorientation of the $GeCl_3^-$ anion take place.

[1] K. Yamada, T. Matsui, T. Tsuritani, T. Okuda, and S. Ichiba, Z. Naturforsch. **45a,** 307 (1990).
[2] K. Yamada, H. Kawaguchi, T. Matsui, T. Okuda, and S. Ichiba, Bull. Chem. Soc. Japan **63,** 2521 (1990).
[3] K. Yamada, S. Funabiki, H. Horimoto, T. Matsui, T. Okuda, and S. Ichiba, Chem. Lett. **1991,** 801.
[4] N. Onoda-Yamamuro, T. Matsuo, and H. Suga, J. Chem. Thermodynamics **23,** 987 (1991).
[5] T. A. Albright, J. K. Burdett, and M. H. Whangbo, Orbital Interactions in Chemistry, P. 258, John Wiley & Sons, New York 1985.
[6] J. I. Musher, Angew. Chem. Int. Ed. **8,** 54 (1969).
[7] K. Yamada, T. Tsuritani, T. Okuda, and S. Ichiba, Chem. Lett. **1989,** 1325.
[8] P. S. Poskozim and A. L. Stone, J. Inorg. Nucl. Chem. **32,** 1391 (1970).
[9] L. M. Dennis and R. E. Hulse, J. Amer. Chem. Soc. **52,** 3553 (1930).
[10] D. A. Everest and H. Terrey, J. Chem. Soc. **1950,** 2282.
[11] D. Messer, Z. Naturforsch. **33b,** 366 (1978).
[12] G. Thiele, H. W. Rotter, and K. D. Schmidt, Z. Anorg. Allg. Chem. **545,** 148 (1987).
[13] A. N. Christensen and S. E. Rasmussen, Acta Chem. Scand. **19,** 421 (1965).
[14] A. Moeller and J. Felsche, J. Appl. Crystallogr. **12,** 617 (1978).
[15] W. Depmeier and A. Moeller, Acta Crystallogr. **B36,** 803 (1980).
[16] F. Izumi, The Rietveld Method, ed. by R. A. Young, Oxford Univ. Press, Oxford 1993.
[17] J. Harada, M. Sakata, S. Hoshino, and S. Hirotsu, J. Phys. Soc. Japan **40,** 212 (1976).
[18] M. Sakuma, J. Harada, M. J. Cooper, and K. D. Rouse, Acta Crystallogr. **A36,** 7 (1989).
[19] O. Knop, R. E. Wasylishen, M. A. White, T. S. Cameron, and M. J. M. Oort, Can. J. Chem. **68,** 4129 (1990).
[20] J. Mizusaki, K. Arai, and K. Fueki, Solid State Ionics **11,** 203 (1983).